

Analysis of the accuracy of GNSS inferred precipitable water vapour against that from a 210 GHz WVR at the H.E.S.S. site

Lott Frans^{1*}, Michael Backes^{1,4}, Heino Falcke², and Tiziana Venturi³

¹*Department of Physics, Chemistry & Material Science, University of Namibia, Private Bag 13301, Windhoek, Namibia*

²*Department of Astrophysics, Institute for Mathematics, Astrophysics and Particle Physics, Radboud University, P.O. Box 9010, 6500 GL Nijmegen, The Netherlands*

³*Istituto di Radioastronomia, Istituto Nazionale di Astrofisica, Via Gobetti 101, 40129 Bologna, Italy*

⁴*Centre for Space Research, North-West University, Private Bag X6001, Potchefstroom 2520, South Africa*

Accepted 18/04/2025. Received 16/04/2025; in original form 29/12/2024

ABSTRACT

The High Energy Stereoscopic System (H.E.S.S.) site and the Gamsberg Mountain have been identified as potential sites for the Africa Millimetre Telescope (AMT). The AMT is poised to observe at millimetre and possibly at submillimetre wavelengths. At these wavelengths, precipitable water vapour (PWV) in the atmosphere is the main source of opacity during observations and therefore needs to be accurately assessed at the potential sites for the AMT. In order to investigate the PWV conditions for the AMT, identical Global Navigation Satellite System (GNSS) stations were installed and used to assess the PWV at the two potential sites. In this study, the accuracy of those PWV measurements by the GNSS stations was assessed by comparing the H.E.S.S. installed GNSS station PWV measurements to that from a 210 GHz Water Vapour Radiometer (WVR) also installed at the H.E.S.S. site. A correlation of 98% and an offset of 0.34 mm was found between the GNSS station and the 210 GHz WVR PWV data when on-site pressure and the Nevada Geodetic Laboratory (NGL) weighted mean temperature (T_m) were used to calculate the GNSS station PWV data. In comparison, the offset reduces to 0.15 mm when on-site derived T_m and pressure were used to calculate the GNSS station PWV. The results show that the GNSS station with on-site meteorological data can be used with high accuracy to reliably determine the PWV conditions at the H.E.S.S. site.

Key words: atmospheric effects – instrumentation – site testing – opacity – submillimetre: general – telescopes

1 INTRODUCTION

The High Energy Stereoscopic System (H.E.S.S.) site (Ohm et al. 2023) is one of two potential sites for the Africa Millimetre Telescope (AMT) with the Gamsberg Mountain being the other option (Frans et al. 2025; Backes et al. 2016). Both the H.E.S.S. site and the Gamsberg Mountain are located within the Khomas Highlands area of Namibia and are approximately 30 km apart. The area is known to have pristine conditions for astronomy and already consists of the H.E.S.S. observatory. The H.E.S.S. observatory observes gamma-rays and consists of an array of five imaging atmospheric Cherenkov telescopes (IACTs) (Ohm et al. 2023; Backes et al. 2023). Although the Gamsberg Mountain has no major observatory yet, the meteorological conditions were previously established to be suitable for astronomy (Sarazin 1995; Frans et al. 2025).

Precipitable water vapour (PWV) is the main source of opacity at millimetre and submillimetre wavelengths as it absorbs emissions at these wavelengths (Smette et al. 2008). Moreover, the presence of PWV causes phase delay on millimetre and submillimetre astronomical signals which may lead to a decline in performance on millimetre and submillimetre long baseline interferometers if not corrected (Nikolic et al. 2013). Backes et al. (2024) conducted a

study in which different instruments at the H.E.S.S. site were used to determine the PWV. The instruments in the study which included of the AERosol RObotic NETwork (AERONET) Holben et al. (1998), Autonomous Tool for Measuring Observatory site COnditions PrE-cisely (Atmoscope) (Fruck et al. 2015), and H.E.S.S. weather station and radiometers (Ohm et al. 2023) all had their biases based on the conditions they take measurements. For example, the AERONET only records during the day during cloudless periods and the CT radiometers only record during photometric nights which results in the PWV from these instruments being biased towards lower values. Furthermore, because of the different conditions and periods under which the instruments record measurements, they could not be properly validated against each other and, therefore, their results could not be verified.

In order to assess the PWV and find the site with the best PWV conditions among the potential sites for the AMT, a Global Navigation Satellite System (GNSS) station was installed at the H.E.S.S. site and the Gamsberg Mountain (Frans et al. 2025). GNSS stations are known to be a viable and reliable alternative to the more conventional use of radiometers in measuring PWV. Combrink (2006) looked into verifying GNSS-derived PWV measurements against those from very-long baseline interferometry (VLBI) observations of the 26-metre Hartebeesthoek radio telescope and a Water Vapour Radiometer (WVR) 2000 at the Hartebeesthoek radio astronomy observatory (HARTRAO). A positive correlation of above

* E-mail: lfrans@unam.na

90% was found between the GNSS-derived PWV measurements and that determined by different methods, such as VLBI observations and WVR 2000 (Combrink 2006). Furthermore, a recent study conducted by Sugiyama et al. (2024) using GNSS station data in the Atacama desert to measure the PWV for submillimetre and millimetre observations proved that GNSS station-derived PWV data could be reliably used for site evaluation and analysis. A comparison between the GNSS station-derived PWV data to scaled radiometer-derived PWV data found the instruments to have a mean offset of 0.64 mm over 15 minutes. Moreover, with the availability of the scaled PWV measurements from the radiometer, a weighted mean temperature (T_m) model with respect to the surface temperature (T_s) was derived for the Atacama. The T_m model allowed the local T_s to be incorporated in the calculation of the GNSS-derived PWV at the Atacama (Sugiyama et al. 2024).

The PWV results at the H.E.S.S. site and Gamsberg Mountain based on the GNSS station measurements by Frans et al. (2025) found that both sites have the potential for millimetre wave astronomy with an overall median PWV of 14.27 mm and 9.25 mm, respectively. During the window of observation for the Event Horizon Telescope (EHT) which typically occurs from March through April, a median PWV value of 16.62 mm and 11.20 mm was determined at the H.E.S.S. site and the Gamsberg Mountain, respectively. The study concluded based on the GNSS PWV data that Gamsberg Mountain had the lowest PWV conditions among the two potential sites. As there was no available site or regional model for T_m , the T_m values used to calculate the PWV of GNSS stations at the H.E.S.S. site and the Gamsberg Mountain were rather interpolated from the European Centre for Medium-Range Weather Forecasts (ECMWF) by the Nevada Geodetic Laboratory (NGL) as opposed to being determined locally on site (Blewitt et al. 2018; Boehm et al. 2006).

According to Frans et al. (2025), MERRA-2 data consist of upper air measurements in addition to satellite and surface measurements assimilated into earth system modelling. The study by Frans et al. (2025) validated MERRA-2 PWV against GNSS station PWV measurements at the H.E.S.S. site and found a 92% correlation and a percentage difference of 7.45% between the two measurements. The difference was attributed to the fact that the MERRA-2 PWV measurements are mainly based on satellite data and also involve interpolation in processing the data to the H.E.S.S. location, which therefore does not take well into account the local on-site conditions (Frans et al. 2025). Studies by Raymond et al. (2021) and Valeria et al. (2024) also looking into potential sites for the next generation (ng) EHT using MERRA-2 data also reported similar discrepancy between PWV from MERRA-2 data and that obtained insitu on some of the potential sites. For example, Valeria et al. (2024) attributed the offset difference at Cerro Paranal in his study to strong local wind conditions due to it being close to the Pacific Ocean.

The above reasons highlight the need of additionally using an instrument such as a radiometer on site as a way of validating any PWV results from a test instrument as oppose to using MERRA-2 data alone. In this study, a 210 GHz WVR was installed insitu at the H.E.S.S. site and used to investigate the accuracy and reliability of the GNSS-derived PWV results by Frans et al. (2025) of both the H.E.S.S. site and the Gamsberg Mountain. Since the T_m used in the calculation of the GNSS PWV was determined through interpolation by the NGL, the study would also look into improving the GNSS station PWV measurement by developing a T_m with



Figure 1. GNSS station (left, in white) installed in 2022 and 210 GHz WVR (right) installed in 2024 to validate GNSS PWV data at the H.E.S.S. site.

respect to on-site T_s for the H.E.S.S. site and the region in general by using the 210 GHz WVR and GNSS station data.

2 METHODS

Since both GNSS stations installed at Gamsberg Mountain and at the H.E.S.S. site are identical in design and the same methods were applied in calculating the PWV from the GNSS stations from both sites, only the PWV from the GNSS station installed at the H.E.S.S. site will be validated. The results of the validation will also apply to the PWV calculated from the GNSS station at the Gamsberg Mountain. The GNSS station at the H.E.S.S. site was installed in September 2022 and has consistently taken data. A 210 GHz WVR that measures opacity was installed in March 2024 alongside the GNSS station (as depicted in Figure 1) in order to validate the PWV measurements from the GNSS station.

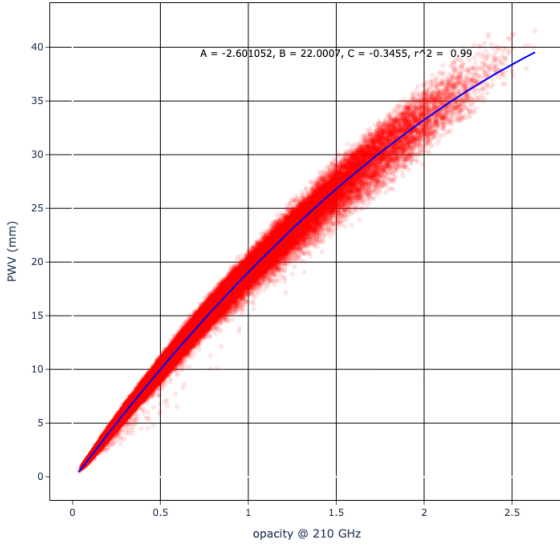
This section will describe the methods applied to the raw data in order to have PWV as a product of both the GNSS station and 210 GHz WVR.

2.1 MERRA-2

Since the 210 GHz radiometer measures the optical depth/opacity τ_0 at zenith at a frequency of 210 GHz, this opacity had to be converted to PWV in order to properly compare with the GNSS PWV data and equally vice versa. To do this, a model of PWV against opacity at 210 GHz was needed at the H.E.S.S. site. For this, MERRA-2 data were used, with the processes applied to acquire the MERRA-2 data at the H.E.S.S. site previously described by Frans et al. (2025). In this study, the MERRA-2 dataset ranges over a 24-years period between 2000 and 2024 with a temporal resolution of 3 hours. The atmospheric models of PWV against opacity at 210 GHz were then created using the 24 years of MERRA-2 data as shown in Figure 2. A polynomial fit of the form,

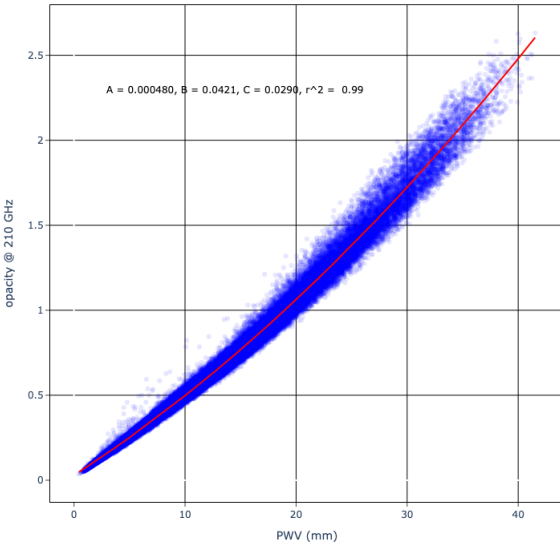
$$y = Ax^2 + Bx + C \quad (1)$$

H.E.S.S. site Model: Opacity vs PWV



(a) The red represents PWV vs opacity at 210 GHz whilst the blue line represents the fit of the form in equation 1 on the data. This model will be used to convert 210 GHz WVR opacity into PWV.

H.E.S.S. site Model: Opacity vs PWV



(b) The blue represents PWV vs opacity at 210 GHz whilst the red line represents the fit of the form in equation 1 on the data. This model will be used to convert GNSS PWV to opacity at 210 GHz.

Figure 2. Models between PWV vs opacity at 210 GHz based on 24 years of MERRA-2 data at the H.E.S.S. site.

was fitted with the coefficients provided in Table 1. The coefficients of determination R^2 , is the measure of how well the model can statistically predict the outcome. Both models for either converting opacity to PWV or visa versa have coefficients of determination of 0.99. This means that the model fits for 99% of the data.

Table 1. Coefficients of the polynomial in equation 1 when fitted to PWV against opacity (τ_0) at 210 GHz at the H.E.S.S. site and its coefficient of determination R^2 .

y	x	A	B	C	r^2
PWV	τ_0	-2.601052 mm	22.0007 mm	-0.3455 mm	0.99
τ_0	PWV	0.000480 mm ⁻²	0.0421 mm ⁻¹	0.029	0.99

2.2 GNSS station

The details of the methods used in this study to retrieve PWV data from GNSS station measurements were previously described by Frans et al. (2025). According to Frans et al. (2025), the PWV data were calculated using the Zenith Total Delay (ZTD) and the T_m provided by the NGL Blewitt et al. (2018) while the pressure used was measured by the MET 4A weather station, which is integrated within the GNSS station. The ZTD is the total delay of signal from satellite at zenith position to the GNSS station receiver and is calculated as the sum of the Zenith Hydrostatic delay (ZHD) and the Zenith Wet Delay (ZWD),

$$ZTD = ZHD + ZWD \quad (2)$$

where the ZHD is then given by,

$$ZHD = (2.2779 \pm 0.0024) \times \frac{P_s}{f(\lambda, H_s)} \quad (3)$$

where P_s is the on site surface pressure in hPa and $f(\lambda, H_s)$ is defined as,

$$f(\lambda, H_s) = 1 - 0.00266 \times \cos(2\lambda) - 0.00028H_s \quad (4)$$

where H_s is the height in metres and λ the latitude of the GNSS station. Given the NGL ZTD products and the calculated ZHD using the pressure P_s measured on site by the MET4A weather station, the ZWD could then be calculated as,

$$ZWD = ZTD - ZHD \quad (5)$$

With the NGL T_m , the PWV was then determined from the ZWD with equation 17 and 16 as described under subsection 3.2. The raw data measurements of the GNSS station are integrated over 30-second intervals but were resampled to 5 minutes intervals by NGL. Figure 3 shows the time series PWV data from the GNSS station at the H.E.S.S. site. Using the coefficients of the relationship derived in Figure 2b tabulated in Table 1 and the relation 1, the PWV was converted in opacity at 210 GHz.

2.3 210 GHz Water Vapour Radiometer

The 210 GHz WVR takes opacity measurements with an integration time that ranges between one measurement per 5 to 15 minutes. According to Hiriart et al. (1997), in the absence of the cosmic background, the antenna temperature T_{ant} of the 210 GHz WVR is given by,

$$T_{ant} = \eta T_{atm} (1 - e^{-\tau}), \quad (6)$$

where η is the coupling factor between the 210 GHz WVR and the antenna, T_{atm} is the atmospheric temperature and τ is the opacity. The total sky temperature T_{sky} of the system is given as the sum of antenna temperature T_{ant} and the receiver noise temperature T_{rec} , then the antenna temperature T_{ant} can then be written as

$$T_{ant} = T_{sky} - T_{rec} \quad (7)$$

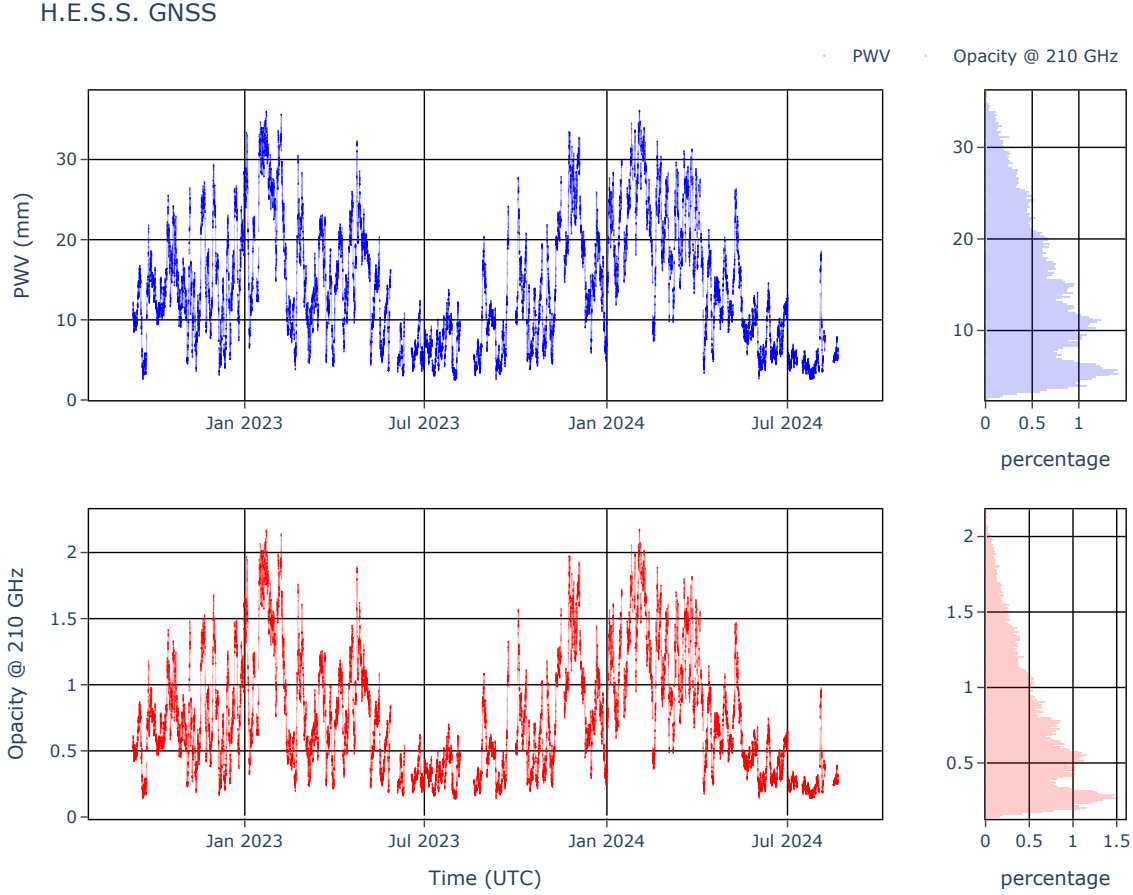


Figure 3. GNSS station PWV and opacity as deduced from the relationship in Figure 2b at the H.E.S.S. site. The NGL T_m and on site pressure was used in the calculation of PWV.

inserting equation 6 into equation 7, we can rewrite equation 7 as,

$$T_{\text{sky}} = \eta T_{\text{atm}} (1 - e^{-\tau}) + T_{\text{rec}}. \quad (8)$$

The temperature load reference is given by,

$$T_{\text{ref}} = \eta T_L + T_{\text{rec}} \quad (9)$$

solving for the receiver temperature T_{rec} in equation 9 and inserting it into equation 8, the expression becomes,

$$T_{\text{ref}} - T_{\text{sky}} = \eta \rho (T_L - T_{\text{atm}} (1 - e^{-\tau})), \quad (10)$$

where ρ is the factor relating the voltage output of the amplifier to the antenna temperature. The comparison between temperature and voltage yields,

$$V_{\text{ref}} - V_{\text{sky}} = \eta \rho (T_L - T_{\text{atm}} (1 - e^{-\tau})). \quad (11)$$

Under an isothermal atmosphere, the ambient temperature around the receiver will be the same everywhere, thus $T_{\text{Load}} \approx T_{\text{atm}}$, this reduces the expression to,

$$V_{\text{ref}} - V_{\text{sky}} = \eta \rho T_{\text{atm}} e^{-\tau}. \quad (12)$$

The optical depth in any direction of the sky can be expressed in terms of the optical depth as zenith τ_0 as,

$$\tau = \tau_0 \sec(z), \quad (13)$$

where z is the zenith angle. Inserting equation 13 into equation 12 and calculating the natural log on both sides of the equation yields,

$$\ln(V_{\text{ref}} - V_{\text{sky}}) = -\tau_0 \sec(z) + \ln(\eta \rho T_{\text{atm}}). \quad (14)$$

For an isothermal atmosphere, there is a linear relationship between the logarithm of the differences of voltages and the zenith distance and can also be shown as,

$$\ln\left(\frac{V_{\text{ref}} - V_{\text{sky}}}{\eta \rho T_{\text{atm}}}\right) = -\tau_0 \sec(z). \quad (15)$$

Therefore, the slope of the linear fit can be determined as the optical depth τ_0 at zenith. Although this method described by [Hiriart et al. \(1997\)](#) was for the 215 GHz WVR, the 210 GHz WVR in this study uses the same method. Figure 4 shows the time series of opacity taken by the 210 GHz WVR and the converted PWV data using the fit in Figure 2a, coefficient in Table 1 and equation 1. It is evident from Figure 4 that there appears to be scatter in the 210 GHz WVR data which seems unphysical.

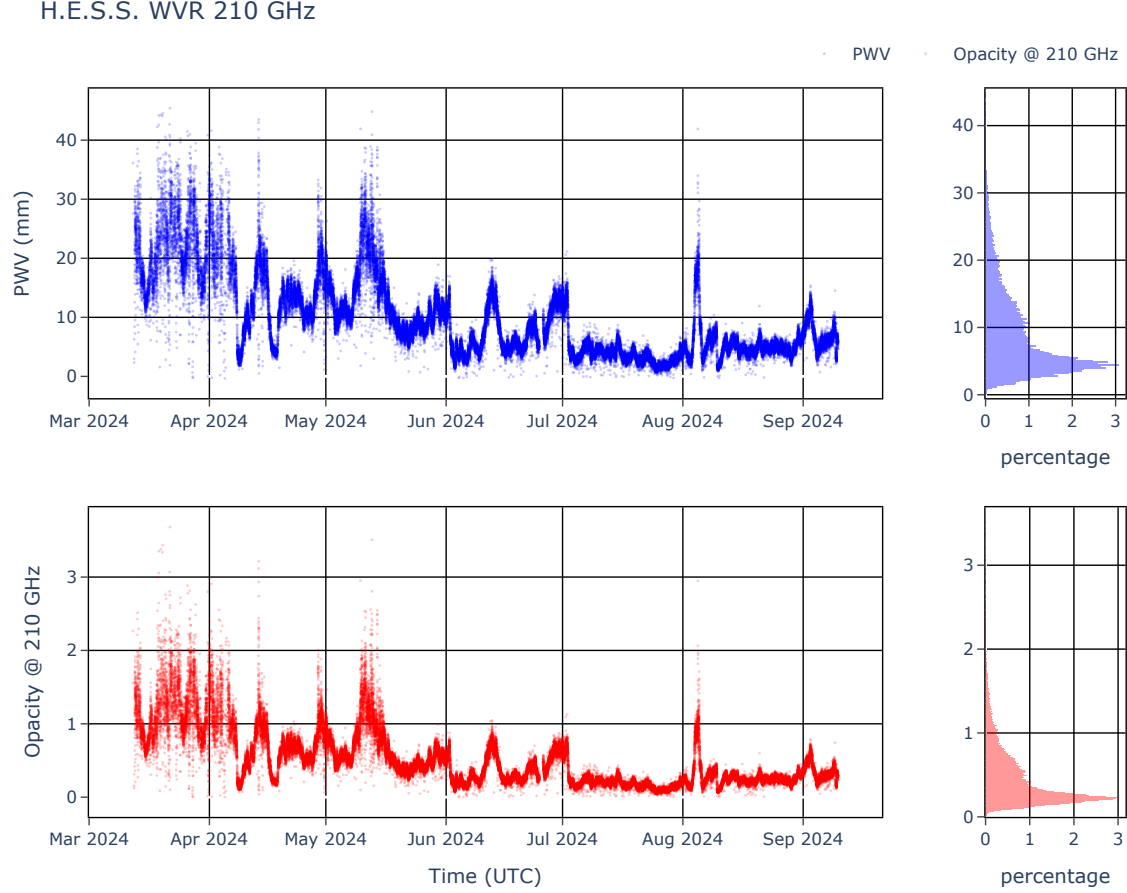


Figure 4. 210 GHz Radiometer opacity and PWV as deduced from Figure 2a at the H.E.S.S. site.

3 RESULTS

3.1 GNSS and 210 GHz Radiometer Comparison

In order to compare the GNSS station and 210 GHz WVR data, both datasets were converted into 15 minutes integration period. The overlapping periods for which data were measured by both instruments were then determined as can be seen in Figure 5. In this study, even though the opacity at 210 GHz can be used to assess the measurements of both instruments, only the PWV was used to determine the accuracy of the two instruments in-line with the evaluation of the PWV results of the study by Frans et al. (2025). It is quite evident from Figure 5 that the GNSS station and the 210 GHz WVR have the same trend in time with the radiometer data seemingly marginally higher. The scatter in the 210 GHz WVR is even more evident as they do not appear in the GNSS station data which is an indication that these points aren't physical but possibly an instrument systematic error. In order to find and remove these scattering data points that account for about 4.75% of the data, a normal distribution of the difference in PWV between the GNSS station and the 210 GHz WVR was found as can be seen in Figure 6a. Simultaneous PWV measurements from both instruments that resulted in a PWV difference greater than 3σ , which is less than -3.52 mm and that greater than 4.21 mm were flagged. This resulted in 95.25% of the data being retained. In doing this, the scatter points in the 210 GHz WVR was

removed as can be seen in Figure 6a. A correlation of 98% was found with a mean offset of 0.35 mm between the instruments. It is quite evident from the fit plot that the two instruments are almost one to one. The resulting data after flagging are shown in Figure 6b, which shows a similar trend in time between the instruments.

3.2 Improving results with on site T_m

The PWV results of the GNSS station can be improved by taking into account the T_m determined locally through on-site measurements rather than through interpolation as done by the NGL. PWV is given by,

$$\text{PWV} = H * \text{ZWD} \quad (16)$$

where ZWD is calculated from equation 2 and H given by,

$$H(T_m) = \frac{10^6}{\rho_w R_w (k'_2 + k_3 T_m^{-1})} \quad (17)$$

where ρ_w is the density of water given as 1000 kg m^{-3} , R_w is the specific gas constant of water vapour, given as $461.4 \text{ J K}^{-1} \text{ kg}^{-1}$ and constants $k'_2 = 22.1 \text{ K hPa}^{-1}$ and $k_3 = 373900 \text{ K}^2 \text{ hPa}^{-1}$ (Sugiyama et al. 2024; Askne & Nordius 1987). The T_m profile of a vertical column of water vapour is conventionally determined with radiosonde

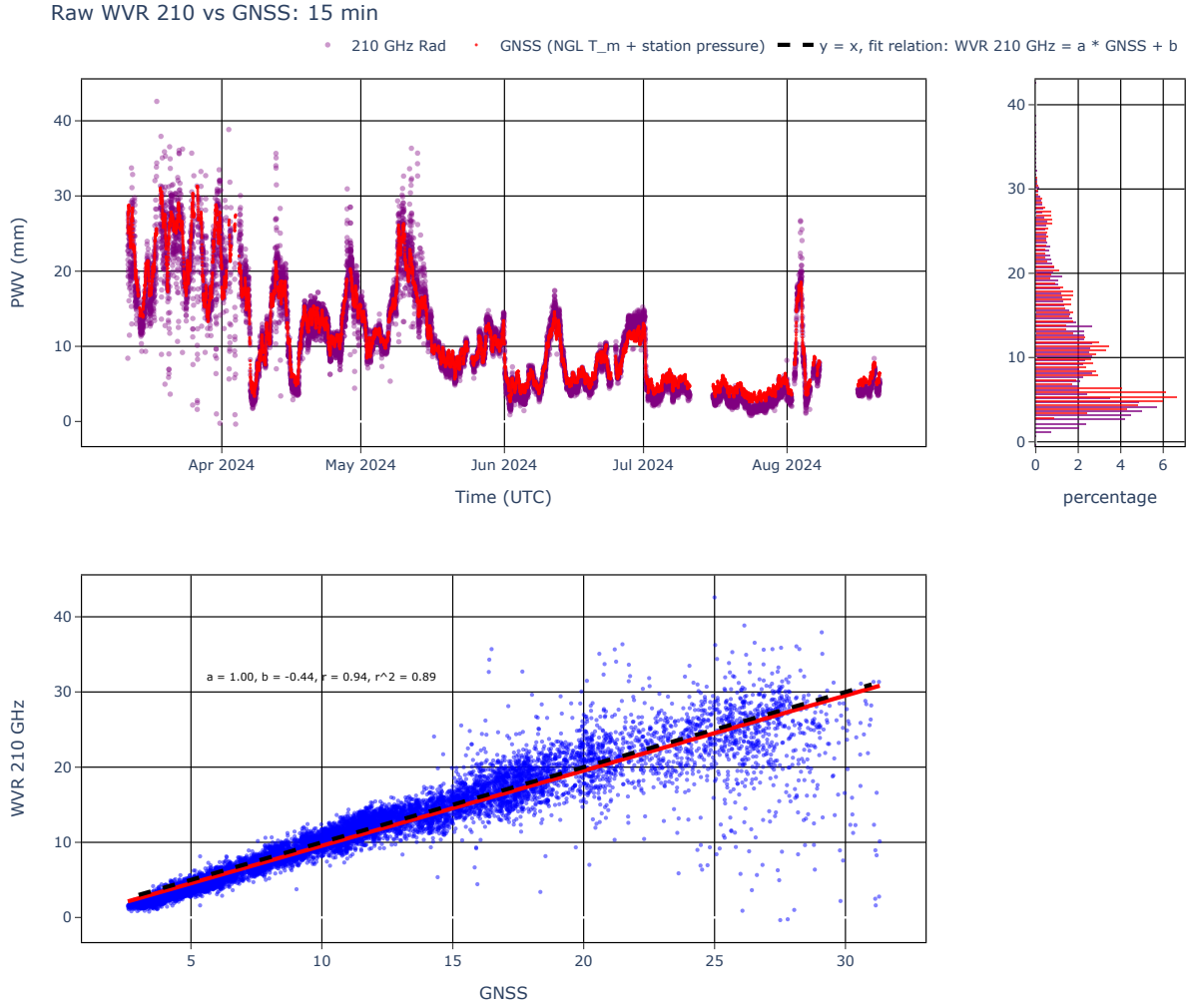


Figure 5. 210 GHz Radiometer and GNSS station PWV measured over the same period at the H.E.S.S. site.

measurements and is given by,

$$T_m = \frac{\int \frac{P_w}{T} dz}{\int \frac{P_w}{T^2} dz} \quad (18)$$

P_w and T are the water vapour pressure and the temperature respectively (Combrink 2006; Sugiyama et al. 2024). Due to the significant effect of the dry bias on the relative humidity measurements in arid regions, it becomes very challenging to measure the T_m using radiosonde (Sugiyama et al. 2024; Otarola et al. 2011). The T_m can also be linearly related to the measured T_s in which it has the form of,

$$T_m = aT_s + b \quad (19)$$

as demonstrated by Sugiyama et al. (2024). Several regional models that relate the T_s to the T_m have been deduced before, such as the Bevis et al. (1992) for the United A States (US), Elhaty et al. (2019) for Egypt (EG), and the model by Sugiyama et al. (2024) for the Atacama. This provides an alternative method for determining the T_m from the ground. The T_m at the H.E.S.S. site was modelled using the methods described in Sugiyama et al. (2024). The 210 GHz WVR provided the PWV data, and the GNSS station provided the

ZTD and T_s for the analysis such as the one described in Sugiyama et al. (2024). Figure A1 provides the fits between the ZWD and the PWV and Figure 7 shows the resulting relationship between the T_m and the T_s . As evident from Figure 7, there were two phases in which there was a positive correlation between the T_m and the T_s till 290 K after which a negative correlation was observed. A piecewise model was then developed for T_m as follow,

$$T_m(T_s) = \begin{cases} 7.03T_s - 1742.64, & \text{if } T_s \leq 290K \\ -2.28T_s + 957.11, & \text{if } T_s > 290K \end{cases} = T_m \quad (20)$$

Using the on site T_s measured by the MET4A weather station on the GNSS station and the model in equation 20, the T_m was then calculated. This now on site T_m were then used to calculate $H(T_m)$ in equation 17 and subsequently the PWV using equation 16. These GNSS station PWV data which are based on insitu pressure and temperature were then compared to the 210 GHz WVR PWV measurements as can be seen in Figure A2.

The use of insitu temperature in the calculation of the PWV slightly improves the results of the GNSS station, as the offset reduced to 0.15 mm compared to 0.34 mm of when the NGL

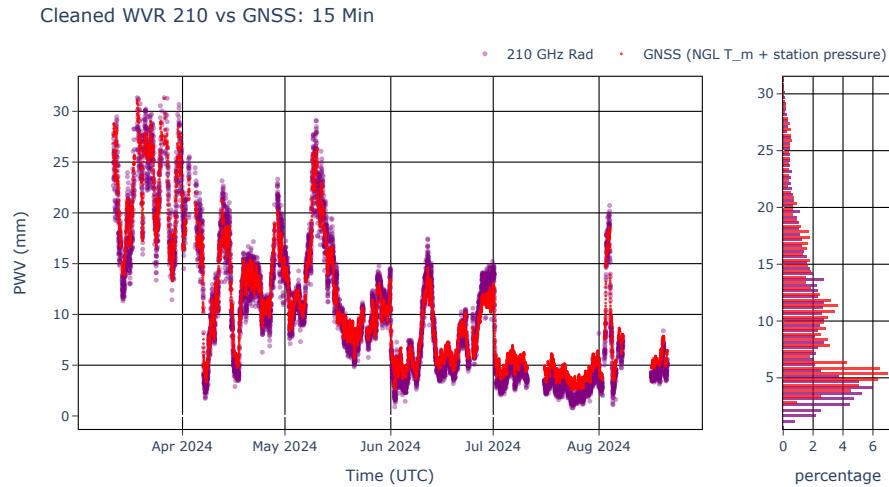
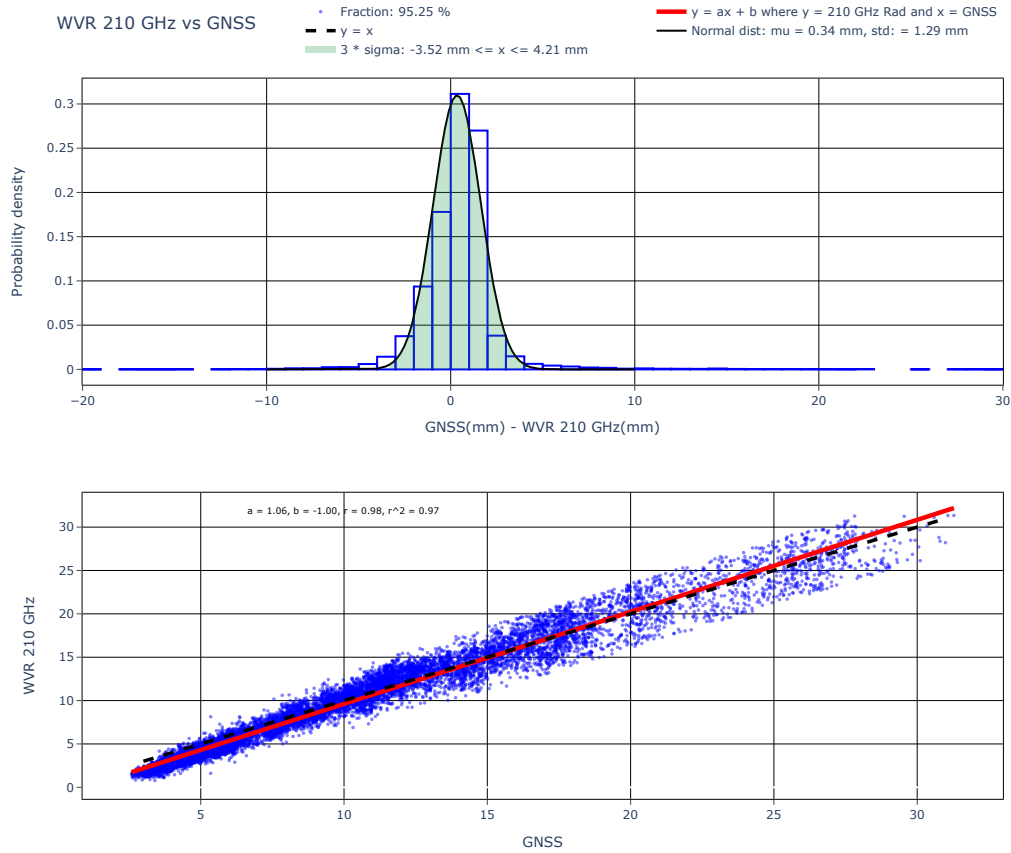


Figure 6. GNSS station and the 210 GHz WVR data after flagging data were the difference of the measurements between the GNSS station and 210 GHz is outside 3σ .

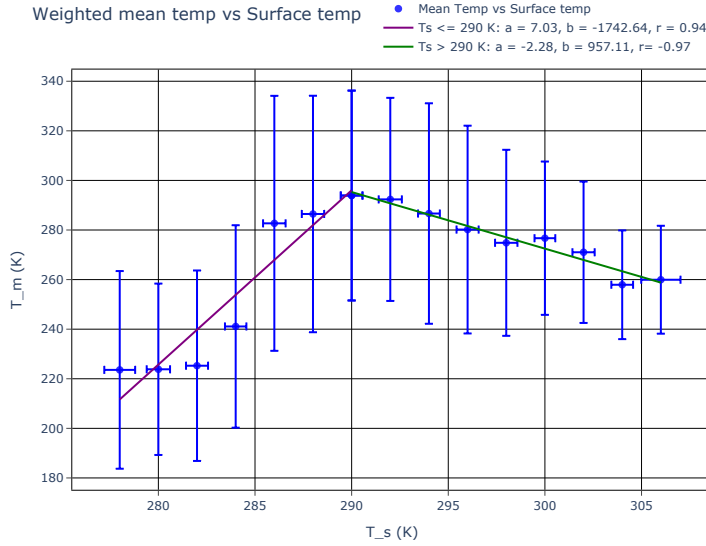


Figure 7. Relationship between T_s and T_m at the H.E.S.S. site.

Table 2. Comparison between 210 GHz WVR and the different GNSS station method.

Method	std [mm]	offset [mm]
NGL T_m , site P_s	1.29	0.34
Site T_m & P_s	1.24	0.15

interpolated mean temperature was used. Table 2 shows the offsets and standard deviation of PWV between the 210 GHz WVR and the GNSS station of when the NGL T_m and when the insitu derived T_m were used. These offsets in Table 2 are much lower when compared to 0.64 mm obtained by Sugiyama et al. (2024) over 15 minutes. The 0.34 mm and 0.15 mm are essentially negligible and suggest the 210 GHz WVR and GNSS station PWV data are one-to-one. The T_m model developed at the H.E.S.S. site shall also apply to the Gamsberg Mountain, as both sites are in the same region and experience the same meteorological conditions.

4 CONCLUSIONS

In this study, GNSS station-derived PWV measurements were validated against 210 GHz WVR-derived PWV measurements at the H.E.S.S. site. The results of this study also apply to the GNSS station at the Gamsberg Mountain as both stations employ similar methods in calculating PWV and are located in the same vicinity with similar meteorological conditions. We have shown a way to convert PWV into opacity at 210 GHz and similarly convert opacity at 210 GHz into PWV by modelling the relationship between PWV and opacity at 210 GHz from MERRA-2 data at the H.E.S.S. site. Using these models, the GNSS station PWV against that from WVR 210 GHz was compared to each other and analysed. We have also managed to develop a T_m model with respect to T_s at the H.E.S.S. site and similarly for the region. A high correlation of 98% was observed between the PWV from the 210 GHz WVR and the GNSS station, with both instruments having similar trends over time. The offset PWV from the 210 GHz WVR and the GNSS was 0.34 mm when on

site pressure from the MET4A was used to calculate the ZHD and the NGL interpolated T_m was used to calculate the PWV. The mean PWV offset between the two instruments improved by reducing to 0.15 mm when the on site T_s was used to calculate the T_m using the model developed in this study, which therefore provides a highly accurate alternative to calculate the PWV with the T_s measured on site. In this study, we showed that the GNSS station can be used with high accuracy to determine the PWV at the H.E.S.S. site and in the region with minimum offset from traditionally utilised instruments such as the 210 GHz WVR. Moreover, we have managed to show that the PWV results based on GNSS station measurements by Frans et al. (2025) is a reliable assessment of the PWV at the H.E.S.S. site and at the Gamsberg Mountain with a minimal offset of 0.34 mm.

ACKNOWLEDGEMENTS

This work was and is supported by multiple institutions including the South African Radio Astronomy Observatory (SARAO) through Dr Roelf Botha and the National Autonomous University of Mexico (UNAM) through Prof. Stanley E. Kurtz and his collaborators in CONACyT-NRF Project 291778./ We also thank the Nevada Geodetic Laboratory (NGL) for processing and presenting the GNSS tropospheric products used in this study. This work has been partially supported by the ERC Synergy Grant *BlackHolistic* and H2020-INFRADEV-2016-1 project 730884 JUMPING-JIVE.

DATA AVAILABILITY

The GNSS, 210 Radiometer and MERRA-2 dataset supporting this study is available from the authors upon reasonable request. Alternatively, GNSS station product data files can be found on the Nevada Geodetic Laboratory link (<http://geodesy.unr.edu/NGLStationPages/stations/GBGA.sta>).

REFERENCES

- Askne, J. & Nordius, H., 1987. Estimation of tropospheric delay for microwaves from surface weather data, *Radio Science*, **22**(3), 379–386.
- Backes, M., Müller, C., Conway, J. E., Deane, R., Evans, R., Falcke, H., Fraga-Encinas, R., Goddi, C., Klein Wolt, M., Krichbaum, T. P., MacLeod, G., Ribeiro, V. A. R. M., Roelofs, F., Shen, Z. Q., & van Langevelde, H. J., 2016. The Africa Millimetre Telescope, in *The 4th Annual Conference on High Energy Astrophysics in Southern Africa (HEASA 2016)*, p. 29.
- Backes, M., Steenkamp, R., Kasai, E., & Matengu, K. K., 2023. The Namibian Multi-wavelength Observatory—Towards Sustained Astronomy in Namibia, in *Space Fostering African Societies*, pp. 31–44, 'Springer New York'.
- Backes, M., Macucule, F. F., & Frans, L. N., 2024. Measurements of Precipitable Water Vapour for the Africa Millimetre Telescope, *PoS, HEASA2023*, 003.
- Bevis, M., Businger, S., Herring, T. A., Rocken, C., Anthes, R. A., & Ware, R. H., 1992. Gps meteorology: Remote sensing of atmospheric water vapor using the global positioning system, *Journal of Geophysical Research: Atmospheres*, **97**(D14), 15787–15801.
- Blewitt, G., Hammond, W., & Kreemer, C., 2018. Harnessing the gps data explosion for interdisciplinary science, *Eos*, **99**(2), e2020943118.
- Boehm, J., Werl, B., & Schuh, H., 2006. Troposphere mapping functions for gps and very long baseline interferometry from european centre for medium-range weather forecasts operational analysis data, *Journal of geophysical research: solid earth*, **111**(B2).
- Combrink, A. Z. A., 2006. *Sensing atmospheric water vapour using the global positioning system*, Ph.D. thesis, University of Cape Town.
- Elhaty, N. M., Abdelfatah, M. A., Mousa, A. E., & El-Fiky, G. S., 2019. Gns meteorology in egypt: Modeling weighted mean temperature from radiosonde data, *Alexandria Engineering Journal*, **58**(2), 443–450.
- Frans, L., Backes, M., Falcke, H., & Venturi, T., 2025. A comparative analysis of GNSS-inferred precipitable water vapour at the potential sites for the Africa Millimetre Telescope, *MNRAS*, **537**(2), 1357–1368.
- Fruck, C., Gaug, M., Ernenwein, J.-P., Mandát, D., Schweizer, T., Häfner, D., Bulik, T., Cieslar, M., Costantini, H., Dominik, M., Ebr, J., Garczarczyk, M., Lorentz, E., Pareschi, G., Pech, M., Puerto-Giménez, I., & Teshima, M., 2015. Instrumentation for comparing night sky quality and atmospheric conditions of cta site candidates, *Journal of Instrumentation*, **10**, P04012.
- Hiriart, D., Goldsmith, P. F., Skrutskie, M. F., & Salas, L., 1997. Atmospheric Opacity at 215 GHz over San Pedro Martir Sierra in Baja California, *Rev. Mex. Astron. Astrofis.*, **33**, 59–68.
- Holben, B. N., Eck, T. F., Slutsker, I., Tanré, D., Buis, J. P., Setzer, A., Vermote, E., Reagan, J. A., Kaufman, Y. J., Nakajima, T., Lavenu, F., Jankowiak, I., & Smirnov, A., 1998. AERONET—A Federated Instrument Network and Data Archive for Aerosol Characterization, *Remote Sensing of Environment*, **66**(1), 1–16.
- Nikolic, B., Bolton, R. C., Graves, S. F., Hills, R. E., & Richer, J. S., 2013. Phase correction for ALMA with 183 GHz water vapour radiometers, *A&A*, **552**, A104.
- Ohm, S., Wagner, S., & H. E. S. S. Collaboration, 2023. Current status and operation of the H.E.S.S. array of imaging atmospheric Cherenkov telescopes, *Nuclear Instruments and Methods in Physics Research A*, **1055**, 168442.
- Otarola, A. C., Querel, R., & Kerber, F., 2011. Precipitable Water Vapor: Considerations on the water vapor scale height, dry bias of the radiosonde humidity sensors, and spatial and temporal variability of the humidity field, *arXiv e-prints*, p. arXiv:1103.3025.
- Raymond, A. W., Palumbo, D., Paine, S. N., Blackburn, L., Córdova Rosado, R., Doeleman, S. S., Farah, J. R., Johnson, M. D., Roelofs, F., Tilanus, R. P. J., & Weintraub, J., 2021. Evaluation of New Submillimeter VLBI Sites for the Event Horizon Telescope, *ApJS*, **253**(1), 5.
- Sarazin, M., 1995. Final Summary Report: Environmental conditions on Potential Observatories, gamsberg astroclimatological summary report, *VLTTRE.ESO.17400*, Accessed 2024-01-19.
- Smette, A., Horst, H., & Navarrete, J., 2008. Measuring the Amount of Precipitable Water Vapour with VISIR, in *2007 ESO Instrument Calibration*

Workshop, p. 433.

Sugiyama, J., Nishino, H., & Kusaka, A., 2024. Precipitable water vapour measurement using GNSS data in the Atacama Desert for millimetre and submillimetre astronomical observations, *Monthly Notices of the Royal Astronomical Society*, **528**(3), 4582–4590.

Valeria, L., Martínez-Ledesma, M., & Reeves, R., 2024. Satellite-based atmospheric characterization for sites of interest in millimeter and sub-millimeter astronomy, *A&A*, **684**, A186.

APPENDIX A: MODELLING THE WEIGHTED MEAN TEMPERATURE

This appendix shows the procedures used to derive the T_m model given by equation 20 for the H.E.S.S. site and the region. It furthermore gives a comparison plot between the 210 GHz WVR PWV data and that obtained from the GNSS station based on the derived insitu T_m .

A1 Calculating the T_m

Following the procedures by Sugiyama et al. (2024), only measurements of PWV, ZWD, and T_s taken at the same time when the relative humidity was greater than 40% were considered during the determination of $H(T_m)$. The ZWD and PWV were partitioned according to T_s as can be seen in Figure A1, with the slope m of the fit relating ZWD and PWV given by,

$$m = \frac{\text{ZWD}}{\text{PWV}} \quad (\text{A1})$$

from equation 16, H can then be calculated from m and is related to m as,

$$H = \frac{\text{PWV}}{\text{ZWD}} = \frac{1}{m} \quad (\text{A2})$$

with H and solving for T_m in equation 17, the T_m was then calculated for the partitioned T_s . The resultant T_m and T_s are shown in Figure 7, from which the relation between T_m and T_s in equation 20 was derived.

A2 Comparison of GNSS station and 210 GHz WVR PWV data when local pressure and T_s are used in calculating GNSS station PWV data

This sections shows the plot comparing the 210 GHz WVR PWV data with those of the GNSS station when insitu pressure and T_s are incorporated into the calculation of the PWV data of the GNSS station. The T_s was used to calculate the T_m using the model given in equation 20.

This paper has been typeset from a \LaTeX file prepared by the author.

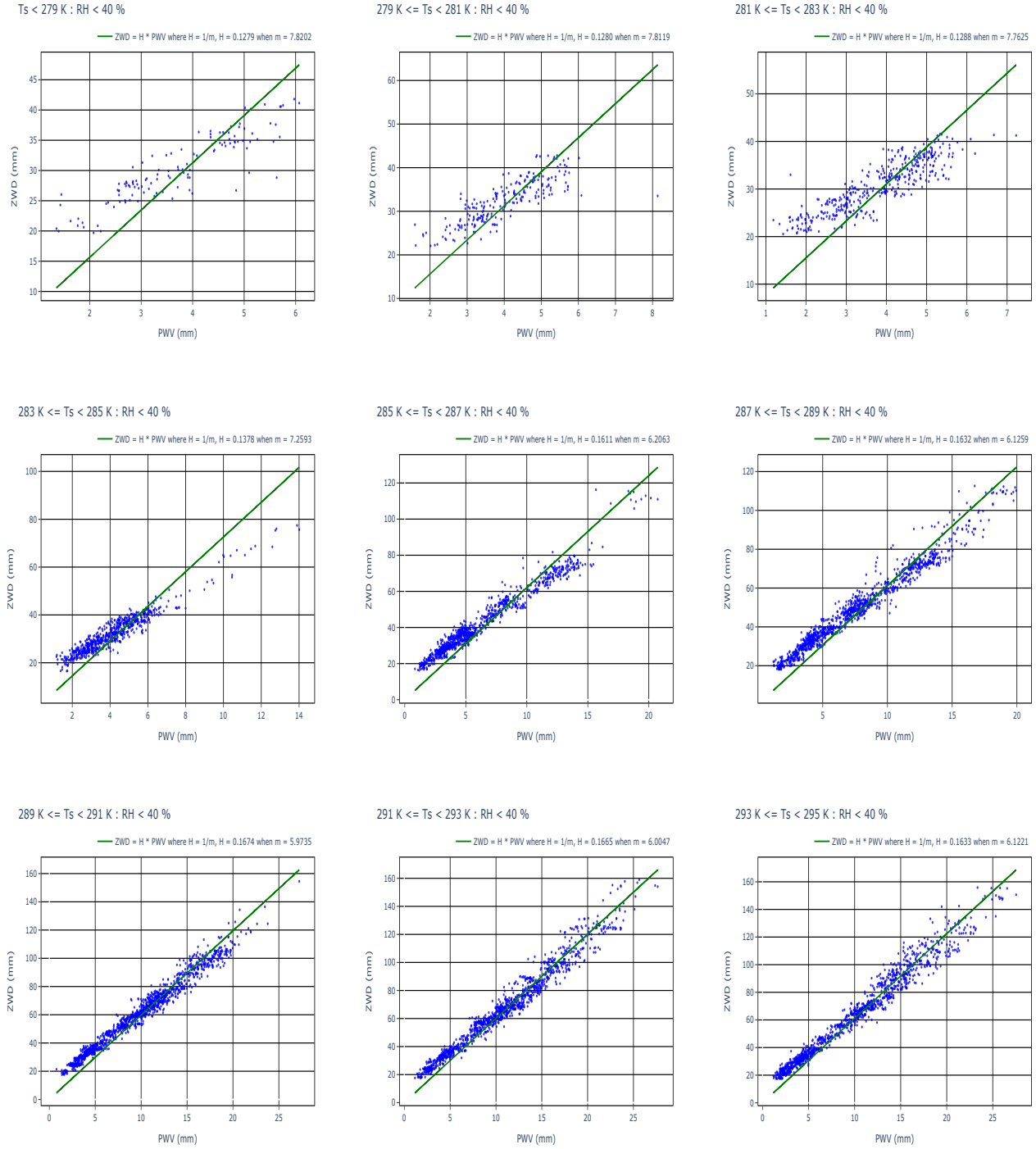


Figure A1. ZWD against PWV at different T_s at the H.E.S.S. site.

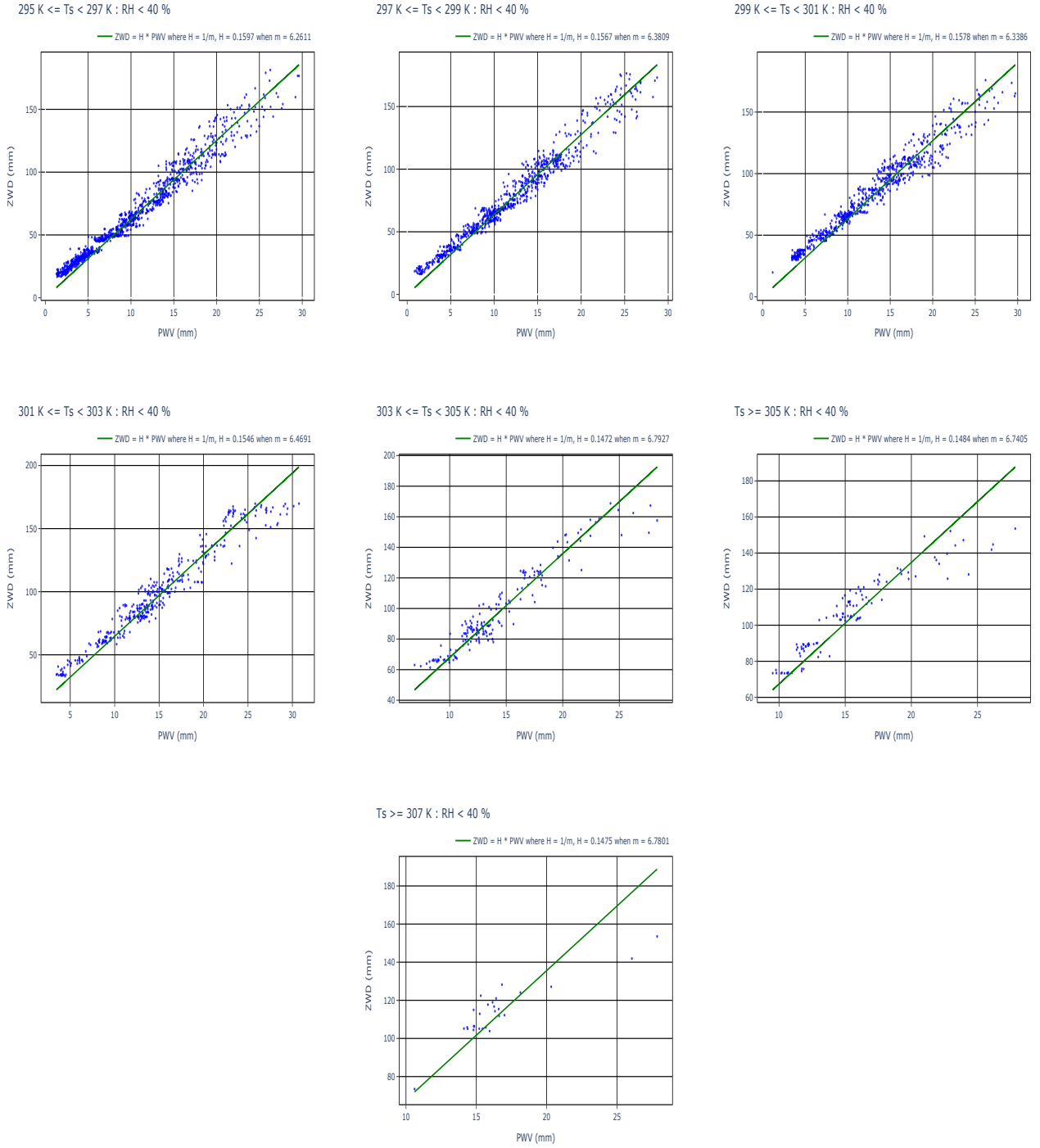


Figure A1. (Continued) ZWD against PWV at different T_s at the H.E.S.S. site.

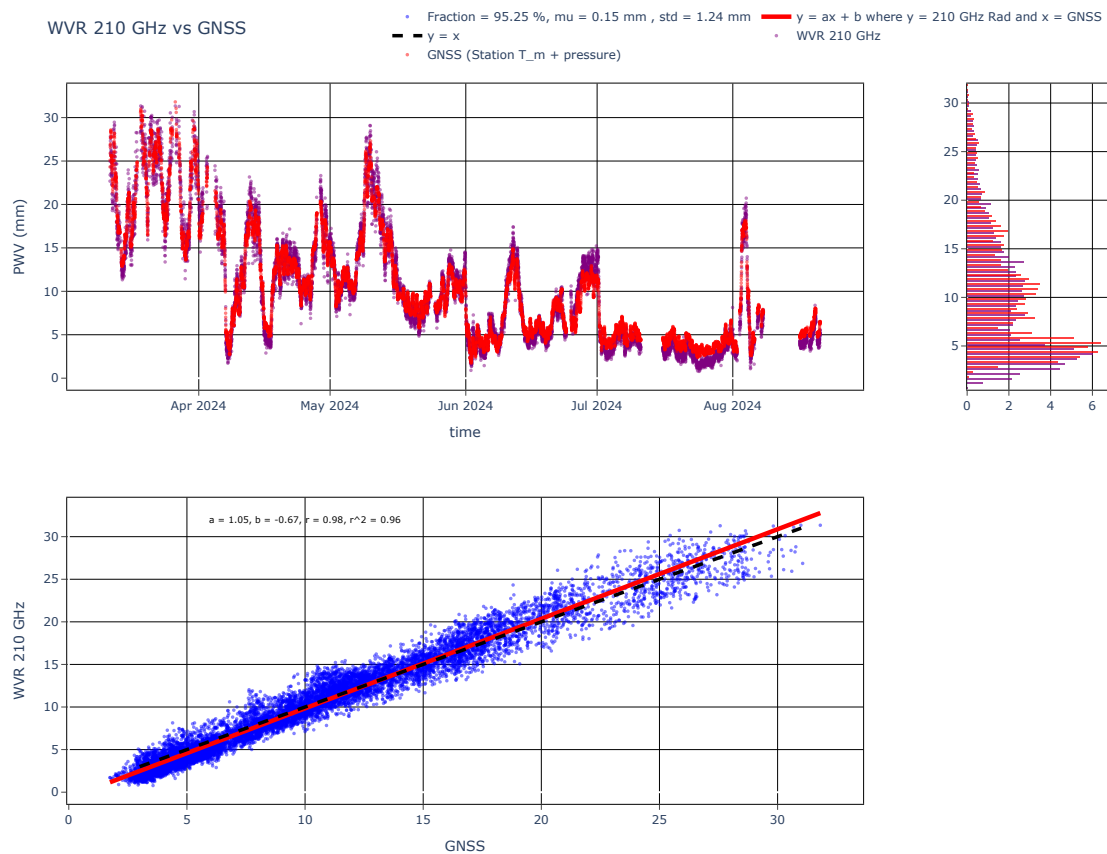


Figure A2. Time series and scatter plots of the resultant PWV from GNSS station when T_m model is used versus PWV from the 210 GHz WVR.